*J. Fluid Mech.* (1990), *vol.* 210, *pp.* 627–645
*Printed in Great Britain*



# On the Lagrangian description of unsteady boundary-layer separation. Part 2. The spinning sphere

By LEON L. VAN DOMMELEN
Department of Mechanical Engineering, FAMU/FSU College of Engineering, PO Box 2175, Tallahasee, FL 32316-2175, USA

(Received 17 March 1989 and in revised form 3 July 1989)

A theory to explain the initial stages of unsteady separation has been proposed by Van Dommelen & Cowley (1990). In the present paper, this theory is verified for the separation process that occurs at the equatorial plane of a sphere or a spheroid which is impulsively spun around an axis of symmetry. A Lagrangian numerical scheme is developed which gives results in good agreement with Eulerian computations, but which is significantly more accurate. This increased accuracy, and a simpler structure to the solution, also allows verification of the Eulerian structure, including the presence of logarithmic terms. Further, while the Eulerian computations broke down at the first occurrence of separation, it is found that the Lagrangian computation can be continued. It is argued that this separated solution does provide useful insight into the further evolution of the separated flow. A remarkable conclusion is that an unseparated vorticity layer at the wall, a familiar feature in unsteady separation processes, disappears in finite time.

## 1. Introduction

In Part 1, Van Dommelen & Cowley (1990) proposed a Lagrangian description for unsteady separation under a wide range of conditions. This theory has been verified in a number of two-dimensional unsteady boundary-layer computations, the first being the one by Van Dommelen & Shen (1980, 1982) for a circular cylinder which is impulsively set into motion in the direction normal to its axis. Yet it seems somewhat unsatisfactory that the verification of basic aspects of the theory should depend solely on two-dimensional unsteady computations, since by necessity their resolution is much lower and their convergence questions more complex than one-dimensional computations. This motivated the present examination of the separation process which occurs at the equatorial plane of a sphere which is impulsively rotated.

This separation process was first described by Banks & Zaturska (1979), who proposed an analytical description in the form of a power series in time. However, Simpson & Stewartson (1982) argued that there would also be higher-order logarithmic terms in the expansion. (Interestingly, Banks & Zaturska 1981 discovered the presence of logarithmic terms in a flow previously studied by Bodonyi & Stewartson 1977, cf. Part 1.) The physical separation process was explained in Lagrangian terms by Van Dommelen (1981), who proposed that separation would cause the boundary layer to divide into an unseparated vorticity layer at the wall and a separated one above it. His proposals agree with the Eulerian expansions of Simpson & Stewartson (1982). While all these studies were only concerned with the

flow in the equatorial plane, numerical solutions for the complete boundary-layer flow were given by Dennis & Ingham (1979) and Van Dommelen (1987). Navier–Stokes solutions were presented by Dennis & Duck (1988).

Except as an example of a basic unsteady separation process, the spinning sphere is also of interest because of its relation to problems in geology and meteorology. It further turns out that the results apply equally well to axially symmetric bodies of general shape, provided that the body is symmetric about the equatorial plane (cf. Part 1 and Banks & Zaturska 1979).

In §4.2 of Part 1, Van Dommelen & Cowley (1990) used their Lagrangian theory to describe separation at a symmetry plane, including the structure close to the symmetry plane. In §§3 and 4 of the present paper, it is verified that the description does indeed apply to the important case of spinning bodies of the type discussed here. For this purpose, in §2 a Lagrangian numerical procedure is described. The Lagrangian procedure is found to be more accurate than the Eulerian Crank–Nicolson scheme of Banks & Zaturska (1979) and the Eulerian box scheme of Simpson & Stewartson (1982). It allows a precise verification of the presence of logarithmic terms in the expansions as proposed by Simpson & Stewartson (1982) (§5). Further, unlike the Eulerian schemes, the Lagrangian computation can be continued beyond the first occurrence of separation without apparent difficulties. The physical meaning of such a solution is not immediately clear, since interaction effects invalidate the equations in the immediate vicinity of the equatorial plane. Yet, in §6 we will argue that our solution can be extrapolated away from the equatorial plane to where the governing equations are still correct. Thus our solution may provide an interesting first glimpse at the continued evolution of an unsteady separated flow. One remarkable result is that the unseparated vortex layer at the wall disappears quickly. In §7 an analytical description for this process is derived which is in good agreement with the numerical data.

## 2. Lagrangian formulation and numerical method

The flow about the spinning sphere is most easily described in a spherical coordinate system in which $x$ is the polar angle measured from the axis of rotation and $y$ is the radial distance from the wall, scaled to eliminate the coefficient of viscosity. The corresponding velocity components are $u$ and $v$, while $w$ denotes the velocity in the azimuthal direction. The radius of the sphere and its angular velocity are scaled to unit values.

In §2 of Part 1, Van Dommelen & Cowley (1990) transformed the boundary-layer equations to Lagrangian 'particle' coordinates $\xi$ and $\eta$ attached to the fluid. By convention, these are taken equal to the values of $x$ and $y$ at the time, $t = 0$, that the sphere initially starts to spin. Thus initially, the equator $x = \frac{1}{2}\pi$ corresponds to $\xi = \frac{1}{2}\pi$ in the Lagrangian coordinate frame. But since the flow velocity is defined as the rate of change of particle position with time, the motion of the particles in the meridional direction, $\dot{x} = u$, vanishes at the equator by symmetry. It follows that the particles initially at the equator stay there for all time: in the Lagrangian domain the equator remains at $\xi = \frac{1}{2}\pi$. The equation for the particle motion $\dot{x} = u$ is, further, trivial at the equator; the equation of interest is its $\xi$-derivative:

$$\dot{x}_{,\xi} = u_{,\xi}, \tag{2.1a}$$

where by convention a subscript comma denotes differentiation with respect to the subsequent subscripts and the dot denotes differentiation with respect to time. At

the equator, the azimuthal Lagrangian momentum equation as given in Part 1 becomes

$$\dot{w} = x_{,\xi}^2 w_{,\eta\eta} + x_{,\xi} x_{,\xi\eta} w_{,\eta}. \tag{2.1b}$$

All terms in the meridional momentum equation vanish by symmetry; the equation of interest is the $\xi$-derivative of the equation at the equator:

$$\dot{u}_{,\xi} = x_{,\xi}^2 u_{,\xi\eta\eta} - x_{,\xi} x_{,\xi\eta} u_{,\xi\eta} + (x_{,\xi\eta}^2 - x_{,\xi} x_{,\xi\eta\eta}) u_{,\xi} - x_{,\xi} w^2. \tag{2.1c}$$

Since $x_{,\xi}$, $u_{,\xi}$, and $w$ are evaluated at the meridional plane $\xi = \frac{1}{2}\pi$, they depend on $\eta$ and $t$ only.

The initial conditions are

$$x_{,\xi}(\eta, 0) = 1, \quad u_{,\xi}(\eta, 0) = 0, \tag{2.1d, e}$$

$$w(\eta, 0) = 0 \quad \text{if} \quad \eta \neq 0, \tag{2.1f}$$

where (2.1*d*) reflects the convention to define $\xi = x$ at $t = 0$. Further (2.1*e*) and (2.1*f*) apply since the initial velocity $(u, v, w)$ is assumed zero when the sphere is first given its spinning motion.

The boundary conditions are

$$x_{,\xi}(0, t) = 1, \quad u_{,\xi}(0, t) = 0, \quad w(0, t) = 1, \tag{2.1g–i}$$

$$x_{,\xi}(\infty, t) = 1, \quad u_{,\xi}(\infty, t) = 0, \quad w(\infty, t) = 0, \tag{2.1j–l}$$

where (2.1*h*) and (2.1*i*) follow from the fact that the particles at the wall, $\eta = 0$, must follow the motion of the wall; for a rotating sphere, the azimuthal velocity at the equator $w = 1$ while the meridional velocity $u$ vanishes uniformly on the sphere. The vanishing of the meridional velocity at the wall also implies that the particles at the wall keep their initial polar position $x = \xi$, hence (2.1*g*) applies. Since in the external flow at $\eta = \infty$ both velocity components $u$ and $w$ vanish, (2.1*j–l*) apply.

The advantage of Lagrangian coordinates arises from the fact that the particle distance from the wall, $y$, occurs only in the continuity equation. The integral form of this equation, given in (2.6) of Part 1, simplifies by symmetry to

$$y = \int_0^\eta \frac{\mathrm{d}\eta'}{x_{,\xi}(\eta', t)}. \tag{2.2}$$

This equation needs to be integrated only at times at which results are desired; it does not affect the numerical solution of (2.1*a–l*). It also turns out that the continuity equation is the first one to become singular, so that numerical difficulties do not arise in the integration of (2.1*a–l*).

The present numerical integration follows the general lines of the procedure of Van Dommelen & Shen (1980). For example, to achieve an effective distribution of mesh points across the boundary layer, an arctangent mapping was used, and the singularity at the impulsive start was eliminated by a further coordinate transformation. The Jacobian (2.2) was integrated using quadratic interpolation for $x_{,\xi}$.

The Lagrangian equations (2.1) were discretisized by means of Crank–Nicolson central finite differences. The resulting implicit finite-difference equations were solved iteratively for $x_{,\xi}$, $w$, and $u_{,\xi}$ respectively by means of the tridiagonal algorithm. The iterations were continued until the error in the finite-difference equivalent of (2.1*a–c*) was less than $3 \times 10^{-8}$; this avoids the possible problems of a termination criterion based on the difference between iterates. To eliminate possible round-off errors, 16-digit numerical precision was used throughout.

| Mesh points... | 129 | 257 | 513 | 1025 | Banks & Zaturska | Simpson & Stewartson |
|---|---|---|---|---|---|---|
| Time step... | 0.025 | 0.0125 | 0.00625 | 0.003125 | | |
| $t_s$ | 4.575676 | 4.575643 | 4.575634 | 4.575632 | 4.5758 | 4.57446 |
| $t_v$ | 5.5418 | 5.5461 | 5.5473 | 5.5476 | | |
| (*a*) $t = 0$ | −0.56415 | −0.56418 | −0.56419 | −0.56419 | −0.564190 | — |
| 0.25 | — | — | — | −1.12666 | −1.12668 | — |
| 1.0 | — | −0.55025 | — | −0.55025 | −0.55029 | −0.5502 |
| 2.0 | — | −0.35771 | −0.35771 | −0.35771 | −0.35773 | −0.3577 |
| 3.0 | — | −0.24414 | −0.24416 | −0.24417 | −0.24418 | −0.2441 |
| 4.0 | −0.14417 | −0.14445 | −0.14452 | −0.14453 | −0.1446 | −0.1445 |
| 4.3 | −0.11450 | −0.11487 | −0.11496 | −0.11498 | −0.1150 | −0.1149 |
| 4.4 | −0.10469 | −0.10508 | −0.10518 | −0.10521 | — | −0.1052 |
| 4.5 | −0.09494 | −0.09537 | −0.09547 | −0.09550 | −0.0955 | −0.0954 |
| 4.52 | −0.09300 | −0.09343 | −0.09354 | −0.09357 | −0.0936 | −0.0935 |
| 4.54 | −0.09106 | −0.09150 | −0.09161 | −0.09164 | −0.0917 | −0.0916 |
| 4.56 | −0.08913 | −0.08958 | −0.08969 | −0.08971 | −0.0897 | — |
| $t_s$ | −0.08761 | −0.08807 | −0.08819 | −0.08821 | — | — |
| 5.0 | −0.04839 | −0.04859 | −0.04866 | −0.04867 | — | — |
| 5.25 | −0.02632 | −0.02653 | −0.02661 | −0.02663 | — | — |
| 5.39 | −0.01424 | −0.01441 | −0.01449 | −0.01452 | — | — |
| 5.47 | −0.00741 | −0.00736 | −0.00745 | −0.00748 | — | — |
| 5.5 | −0.00527 | −0.00463 | −0.00472 | −0.00475 | — | — |
| 5.537 | — | — | −0.00115 | −0.00118 | — | — |
| (*b*) $t = 0$ | −0.40990 | −0.41000 | −0.41002 | −0.41003 | −0.41003 | — |
| 0.25 | — | — | — | −0.20527 | −0.20527 | — |
| 1.0 | — | −0.41855 | — | −0.41858 | −0.41855 | −0.4186 |
| 2.0 | — | −0.63387 | −0.63396 | −0.63398 | −0.63395 | −0.6340 |
| 3.0 | — | −0.89600 | −0.89618 | −0.89622 | −0.89619 | −0.8963 |
| 4.0 | −1.40385 | −1.40486 | −1.40513 | −1.40520 | — | −1.4058 |
| 4.3 | −1.71445 | −1.71522 | −1.71543 | −1.71549 | — | −1.7166 |
| 4.4 | −1.85470 | −1.85794 | −1.85810 | −1.85814 | — | −1.8594 |
| 4.5 | −2.03105 | −2.03121 | −2.03127 | −2.03128 | — | −2.0330 |
| 4.52 | −2.07037 | −2.07043 | −2.07047 | −2.07048 | — | −2.0722 |
| 4.54 | −2.11148 | −2.11143 | −2.11143 | −2.11144 | — | −2.1133 |
| 4.56 | −2.15450 | −2.15432 | −2.15429 | −2.15429 | — | — |
| $t_s$ | −2.18962 | −2.18927 | −2.18920 | −2.18918 | — | — |
| 5.0 | −4.132 | −4.110 | −4.104 | −4.103 | — | — |
| 5.25 | −9.026 | −8.903 | −8.873 | −8.865 | — | — |
| 5.39 | −22.34 | −21.63 | −21.45 | −21.41 | — | — |
| 5.5 | −151 | −129 | −125 | −124 | — | — |
| 5.537 | — | — | −1231 | −1171 | — | — |

TABLE 1. The wall shear at the equatorial plane of the spinning sphere. (*a*) Values of the wall shear $w_{,y}$ and (*b*) values for the wall shear gradient $u_{,xy}$.

Thus the major source of numerical inaccuracy should be the truncation error. To take account of this error, computations were performed at the four meshes listed in table 1, which compare favourably to the meshes used in the Eulerian computations.

In contrast to the Eulerian calculations, no Richardson extrapolation was used. But if desired, it may be noted that the Lagrangian solution should provide a much better basis for repeated Richardson extrapolation than the Eulerian schemes. The reason is the smoothness of the Lagrangian solution discussed in the next section.

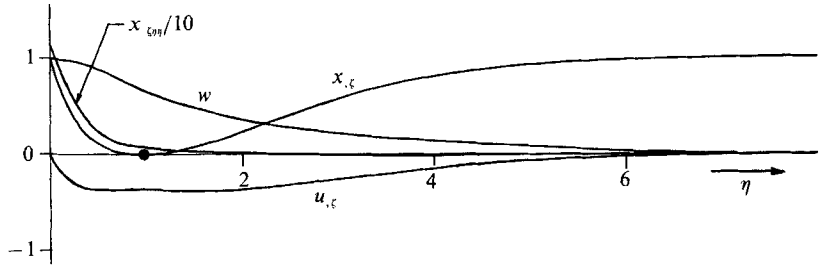


FIGURE 1. Lagrangian boundary-layer profiles in the equatorial plane of the impulsively spun sphere at the time $t_s = 4.575632$ that separation starts. Here $w$ is the azimuthal velocity component and $u_{,\xi}$ the Lagrangian gradient of the meridional velocity $u$. Further, $x_{,\xi}$ is the Lagrangian gradient of the polar particle position $x$. The separation particle $\eta_s = 0.97188$ is indicated by a solid dot. The condition of vanishing $x_{,\xi}$ implies a singular Eulerian velocity profile.

| | $129 \times 0.025$ | $257 \times 0.0125$ | $513 \times 0.00625$ | $1025 \times 0.003125$ | Simpson & Stewartson |
|---|---|---|---|---|---|
| $t = 4$ | 0.035150 | 0.035127 | 0.035121 | 0.035120 | 0.0352 |
| 4.3 | 0.017546 | 0.017511 | 0.017501 | 0.017499 | 0.0176 |
| 4.4 | 0.011318 | — | 0.011243 | 0.011240 | 0.0112 |
| 4.5 | 0.00504 | 0.00491 | 0.00488 | 0.00486 | 0.0045 |
| 4.52 | 0.00381 | 0.00362 | 0.00359 | 0.00359 | 0.0027 |

TABLE 2. The quantity $|u_{,x}|^{-1}_{\max} - (t_s - t)^{-1}$ according to the present four meshes and according to Simpson & Stewartson (1982)

## 3. Separation structure

In solving the problem specified by (2.1), (2.2) in Eulerian coordinates, Banks & Zaturska (1979) discovered that the boundary-layer thickness becomes infinite at some finite time $t_s$. According to Sears & Telionis (1975), such singularities in a classical boundary-layer solution indicate separation. The singularity should be understood to mean that the local motion away from the wall becomes too strong to be described with boundary-layer scalings. As an example, Elliott, Cowley & Smith (1983) show that the interactive stage of unsteady two-dimensional separation occurs at a boundary-layer thickness $O(Re^{-\frac{5}{11}})$, rather than the classical $O(Re^{-\frac{1}{2}})$.

The separation processes proposed in §4.3 of Part 1 are characterized by non-singular solutions $x_{,\xi}$, $u_{,\xi}$, and $w$ to the Lagrangian boundary-layer equations (2.1). Singular behaviour should occur only in the continuity equation (2.2), caused by vanishing of $x_{,\xi}$ inside the boundary layer. Such behaviour results in infinite values of the particle position $y$, leading to the infinite boundary-layer thickness observed in the Eulerian computations.

The present numerical results, such as table 1 and figure 1, do show that the Lagrangian $x_{,\xi}$, $u_{,\xi}$ and $w$ profiles remain regular, and that $x_{,\xi}$ becomes zero. The first zero occurs at a point s located at $\eta_s = 0.97188$ at time $t_s = 4.575632$. This time is in excellent agreement with the time that the Eulerian solution becomes singular, 4.5758 according to Banks & Zaturska (1979) or 4.57446 according to Simpson & Stewartson (1982). (Values of the computational quantity used by Simpson & Stewartson to find the separation time are listed in table 2.) Yet, unlike the Eulerian

| $t$ | $\eta$ | $w$ | $u_{,\xi}$ | $x_{,\xi\eta\eta}$ | $u_{,\xi\eta}$ | $x_{,\xi\eta\eta\eta}$ |
|---|---|---|---|---|---|---|
| $t_s$ | 0.97189 | 0.672593 | −0.369784 | 0.689301 | −0.04000 | −1.1328 |
| | 0.97185 | 0.669262 | −0.369789 | 0.689116 | −0.04019 | −1.1291 |
| | 0.97186 | 0.669249 | −0.369789 | 0.689064 | −0.04026 | −1.1276 |
| | 0.97188 | 0.669240 | −0.369790 | 0.689062 | −0.04026 | −1.1274 |
| $t$ | $\eta_1$ | $w_1$ | $u_{,\xi_1}$ | $\eta_2$ | $w_2$ | $u_{,\xi_2}$ |
| 5 | 0.41478 | 0.92405 | −0.46260 | 1.81402 | 0.39848 | −0.40755 |
| | 0.41507 | 0.92389 | −0.46196 | 1.81422 | 0.39838 | −0.40763 |
| | 0.41513 | 0.92385 | −0.46180 | 1.81426 | 0.39837 | −0.40764 |
| | 0.41515 | 0.92385 | −0.46176 | 1.81427 | 0.39837 | −0.40764 |
| 5.25 | 0.28209 | 0.97193 | −0.7501 | 2.09452 | 0.33781 | −0.41589 |
| | 0.28281 | 0.97167 | −0.7454 | 2.09465 | 0.33776 | −0.41597 |
| | 0.28300 | 0.97159 | −0.7442 | 2.09468 | 0.33774 | −0.41599 |
| | 0.28304 | 0.97158 | −0.7439 | 2.09469 | 0.33774 | −0.41600 |
| 5.39 | 0.20346 | 0.98922 | −1.394 | 2.23830 | 0.31096 | −0.41926 |
| | 0.20473 | 0.98900 | −1.370 | 2.23844 | 0.31089 | −0.41937 |
| | 0.20494 | 0.98900 | −1.364 | 2.23846 | 0.31088 | −0.41939 |
| | 0.20500 | 0.98900 | −1.363 | 2.23846 | 0.31088 | −0.41939 |
| 5.47 | 0.1435 | 0.99643 | −3.025 | 2.31751 | 0.29725 | −0.42090 |
| | 0.1463 | 0.99610 | −2.874 | 2.31763 | 0.29720 | −0.42101 |
| | 0.1469 | 0.99606 | −2.841 | 2.31765 | 0.29719 | −0.42103 |
| | 0.1470 | 0.99605 | −2.834 | 2.31766 | 0.29718 | −0.42103 |
| 5.5 | 0.1124 | 0.99831 | −5.33 | 2.34681 | 0.29231 | −0.42152 |
| | 0.1161 | 0.99811 | −4.89 | 2.34686 | 0.29231 | −0.42158 |
| | 0.1171 | 0.99805 | −4.78 | 2.34686 | 0.29231 | −0.42160 |
| | 0.1173 | 0.99804 | −4.75 | 2.34687 | 0.29231 | −0.42161 |
| 5.537 | — | — | — | — | — | — |
| | — | — | — | — | — | — |
| | 0.0573 | 0.99978 | −24.0 | 2.38259 | 0.28648 | −0.42227 |
| | 0.0581 | 0.99977 | −23.2 | 2.38259 | 0.28648 | −0.42228 |

TABLE 3. Stationary point trajectory (figure 6) and corresponding Lagrangian quantities for the four increasingly fine meshes of table 1. Note that these values do not Richardson extrapolate; they were found from second-order interpolation between the mesh points. However, at the time $t_s$ of first separation, the stationary point happens to fall nearly exactly on a mesh point of the finest two meshes. The four values for each quantity are in order of increasing accuracy.

separation profiles, the Lagrangian profiles of figure 1 do not show any sign of singular behaviour.

The vanishing of $x_{,\xi}$ leads to a singular solution of the continuity equation (2.2) for the $y$-position of the particles. To find the structure of this singularity, $x_{,\xi}$ can be expanded in a finite Taylor series expansion around the point s:

$$x_{,\xi} = \tfrac{1}{2}x_{,\xi\eta\eta}(\eta', t_s)\,\delta\eta^2 + u_\xi(\eta, t')\,\delta t. \tag{3.1a}$$

Since $x_{,\xi}$ has its first zero at time $t_s$, it must be a minimum, with $x_{,\xi}$ still positive elsewhere, so that there is no term linear in $\delta\eta$ in the Taylor series. The generalized form of this condition was given in §4.3 of Part 1. The precise requirement for the Taylor series (3.1 $a$) to be valid is that the appearing derivatives are well-defined, i.e. continuous near the point s. The computed $x_{,\xi\eta\eta}$ and $u_{,\xi}$ profiles at time $t_s$, figure 1, show no sign of singular behaviour at point s, and prove highly accurate according to comparisons for varying mesh size. As an example, table 3 lists the convergence of the values of $x_{,\xi\eta\eta}$ and $u_{,\xi}$ at the point s, along with their $\eta$-derivatives.

The Taylor series expansion (3.1*a*) may be substituted into the continuity equation (2.2) to find the vertical position $y$ of the particles:

$$Y \equiv |\delta t|^{\frac{1}{2}} y = \frac{2}{\beta}\left(\arctan \frac{x_{\xi\eta\eta}(\eta-\eta_s)}{\beta|\delta t|^{\frac{1}{2}}} + \tfrac{1}{2}\pi\right) + o(1), \tag{3.1b}$$

$$\beta = (-2x_{\xi\eta\eta}u_\xi)^{\frac{1}{2}}, \quad \eta = O(1). \tag{3.1c, d}$$

Here, the omission of the subscript comma indicates that the value of the derivative at the point s is meant. This paper follows the Eulerian definitions of the constants closely; in terms of the notation used in Part 1, $\beta$ corresponds to $\sqrt{3}\gamma\beta_2$, and $\beta/x_{\xi\eta\eta}$ to $\beta_0\beta_2$. Our value for the constant $\beta = 0.71387$, table 3, is in good agreement with the 0.71 of Banks & Zaturska (1979) and the 0.712 of Simpson & Stewartson (1982). Except for the difference in the definition of the constants, the vertical position of the particles (3.1*b*) is identical to the elliptic function given in (4.9) of Part 1 when evaluated at the symmetry plane. However, the derivation given here is mathematically a bit more rigorous since no asymptotic expansions were used.

Figure 2 shows Eulerian velocity profiles in terms of the above scaled coordinate $Y$ and the scaled Eulerian velocity gradient:

$$G = -|\delta t|\, u_{,x}, \quad u_{,x} = \frac{u_{,\xi}}{x_{,\xi}}. \tag{3.2a, b}$$

In these velocity profiles, the particles $\eta < \eta_s$ are found in a wall layer near $Y = 0$ (see (3.1*b*)); similarly the particles $\eta > \eta_s$ are located in a separating layer near $\beta Y = 2\pi$. The part $0 < \beta Y < 2\pi$ comprises most of the Eulerian velocity profile, yet it corresponds to only a small vicinity $\delta\eta = O(|\delta t|^{\frac{1}{2}})$ of the point s in the Lagrangian profile.

The last observation implies that for $0 < \beta Y < 2\pi$, a Taylor series expansion for the Lagrangian solution is applicable. The Lagrangian coordinate $\eta$ may subsequently be eliminated in favour of $Y$ by means of (3.1*b*) to find asymptotic expressions for the Eulerian velocity profiles:

$$w \sim w_s, \tag{3.3a}$$

$$u_{,x} \sim -|\delta t|^{-1}\tfrac{1}{2}(1-\cos(\beta Y)). \tag{3.3b}$$

To the order of approximation shown so far, the velocity profiles may alternatively be found from the expressions given in §4 of Part 1.

The scaling (3.1*b*) of the variable $Y$ compensates for the rapid expansion of the region of particles near $\eta_s$. This scaling leads to the apparent thinning of the wall layer and the separating layer in the velocity profiles of figure 2: in terms of the original coordinate $y$, these two layers remain of finite thickness.

To find the separation structure to higher order of approximation, it is more convenient to replace the finite Taylor series expansion (3.1*a*) in favour of a formal matched asymptotic expansion. The proper inner $\eta$-coordinate $E$ near the particle $\eta_s$ can easily be found by applying Van Dyke's (1975) guiding principles: clearly the reason for the non-uniformity in the continuity equation (2.2) is the vanishing of $x_{,\xi}$ at the particle $\eta_s$. Removal of this non-uniformity requires that the time-dependent term in the Taylor series expansion (3.1*a*) is retained in the inner region. On the other hand, the matching with the wall and separating layers can only be done when the

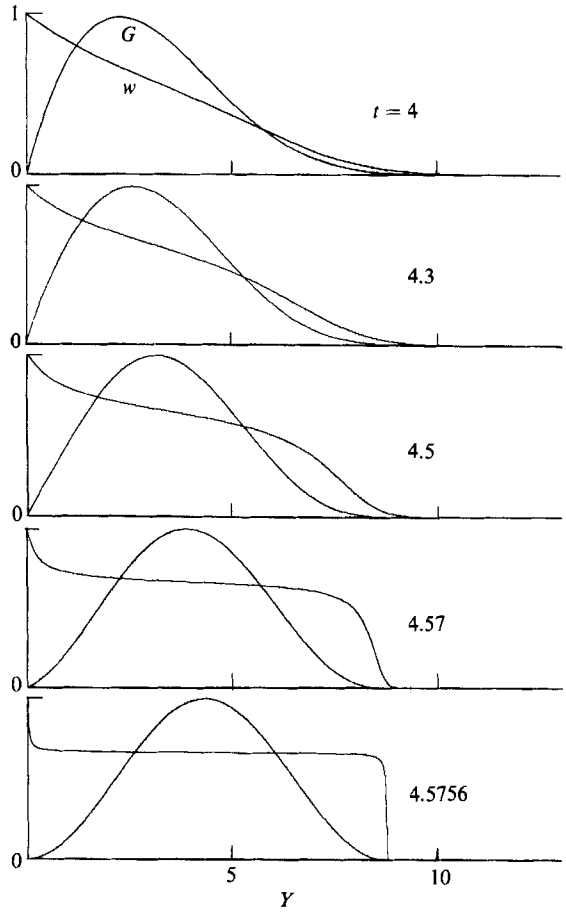


FIGURE 2. Eulerian velocity profiles when the time of first separation is approached. $Y$ is a scaled distance (3.1$b$) from the wall and $G$ is the scaled meridional velocity gradient $u_{,x}$ defined in (3.2$a$). Comparison of the profiles of the azimuthal velocity $w$ with the one of figure 1 shows that near separation most of the Eulerian velocity profile corresponds to only a small vicinity of the stationary point $\eta_s$ of the Lagrangian profile figure 1.

second-order term is retained also. Therefore an inner coordinate $E^*$ will be defined as

$$\delta\eta \equiv |\delta t|^{\frac{1}{2}} \frac{\beta}{x_{\xi\eta\eta}} E^*, \tag{3.4a}$$

which is also consistent with (3.1$b$). An inner dependent variable $\Delta Y^*$ can be defined as

$$y \equiv \frac{Y}{|\delta t|^{\frac{1}{2}}} \equiv y_s(t) + \frac{1}{|\delta t|^{\frac{1}{2}}} \frac{2}{\beta} \Delta Y^*, \tag{3.4b}$$

where $y_s(t)$ denotes the vertical distance of the particle $\eta_s$ from the wall, a distance which has been subtracted in order to avoid the appearance of logarithmic terms in the Lagrangian inner expansions.

With the inner scalings known, it is a simple matter to integrate (2.2) to find the particle position:

$$\Delta Y^* = \arctan(E^*) + |\delta t|^{\frac{1}{2}}\left(-\beta B \ln(1+E^{*2}) + \frac{(\beta B + C)E^{*2}}{1+E^{*2}}\right) + \ldots, \tag{3.5a}$$

$$\beta \equiv (-2x_{\xi\eta\eta}u_\xi)^{\frac{1}{2}}, \quad B \equiv \frac{x_{\xi\eta\eta\eta}}{6x_{\xi\eta\eta}^2}, \quad C \equiv \frac{u_{\xi\eta}}{\beta}. \tag{3.5b–d}$$

The Eulerian velocity profiles are found by a Taylor series expansion of the Lagrangian profiles, followed by the elimination of the Lagrangian coordinate using (3.5*a*):

$$G \sim \tfrac{1}{2}(1+\cos 2\Delta Y^*) + |\delta t|^{\frac{1}{2}}\beta B \sin(2\Delta Y^*)\ln(\tfrac{1}{2}(1+\cos 2\Delta Y^*)) + \ldots, \tag{3.6a}$$

$$w \sim w_s + |\delta t|^{\frac{1}{2}}\frac{\beta w_\eta}{x_{\xi\eta\eta}}\tan\Delta Y^*. \tag{3.6b}$$

The asymptotic value of the azimuthal velocity $w_s$ is easily found by evaluating the Lagrangian $w$-profile figure 1 at the separation point s. The various derivatives are found by numerical differentiation of the Lagrangian separation profiles and evaluation at point s. Since in general the point s does not coincide exactly with a mesh point, interpolation is needed in the evaluation.

The above Eulerian results agree with the inner structure of Banks & Zaturska (1979) as modified by Simpson & Stewartson (1982).

## 4. The wall and separating layers

The inner solution derived in the previous section can be matched below, at $E^* = -\infty$, to a wall layer of particles $\eta < \eta_s$, and above, at $E^* = \infty$, to a separating layer of particles $\eta > \eta_s$. In the wall layer, all variables including the particle position $y$ are non-singular since the integral (2.2) does not involve the singular point $\eta_s$. The asymptotic description of the wall layer is therefore a Taylor series expansion in time (cf. (3.24) in Part 1):

$$(x_{,\xi}, u_{,\xi}, w, y) = \sum_{n=0}^{\infty}\frac{1}{n!}|\delta t|^n (x_{,\xi}^{(n)}(\eta), u_{,\xi}^{(n)}(\eta), w^{(n)}(\eta), y^{(n)}(\eta)) \quad \text{for} \quad \eta < \eta_s. \tag{4.1a, b}$$

It is not possible to add singular terms of the general form $|\delta t|^\alpha \ln|\delta t|$ to this expansion, for substitution into the Lagrangian equations (2.1) and (2.2) would lead to inconsistencies.

The Eulerian asymptotic expansion of the wall layer is found by formal elimination of $\eta$ in favour of $y$:

$$(u_{,x}, v, w) = \sum_{n=0}^{\infty}\frac{1}{n!}|\delta t|^n (u_{,x}^{*(n)}(y), v^{*(n)}(y), w^{*(n)}(y)) \quad \text{for} \quad y = O(1). \tag{4.2a, b}$$

The vertical velocity component $v$ is simply the integral of $u_{,x}$ with respect to $y$.

Substitution of the expansions (4.1) into the equations of motion determines the $x_{,\xi}^{(n)}$, $u_{,\xi}^{(n)}$, $w^{(n)}$, $(n > 0)$, and the $y^{(n)}$, $(n \geqslant 0)$, in terms of the separation profiles $x_{,\xi}^{(0)}$, $u_{,\xi}^{(0)}$, and $w^{(0)}$. However, self-consistency does not pose constraints on the shape of the separation profiles themselves. This does not necessarily mean that any separation profile will correspond to a realistic solution: if we use the linear heat equation as a model, a velocity profile can only correspond to a solution at earlier times if its

Fourier transform decays sufficiently rapidly with the wavenumber. For this simple model problem, suitable profiles, which are arbitrary close to incorrect solutions, can be found by truncating the Fourier transforms of the incorrect profiles at large wavenumbers.

To examine whether modification of the velocity profile in the wall layer is indeed possible, the computations were repeated for the case in which the sphere is gradually brought to a halt in the time interval $4 < t < 4.5 (< t_s)$. The choice $t = 4$ was made because a crude preliminary estimate suggested that $t_s - 4$ was too short a time interval for diffusion to reach the particle $\eta_s$. The velocity change was prescribed as

$$w(0,t) = \frac{1}{1+\exp\left(2T/(1-T^2)\right)}, \quad T \equiv \frac{(t-4.25)}{0.25}. \tag{4.3a, b}$$

As can be expected, the results in figure 3 show that the Lagrangian separation profiles are dramatically altered near the wall. Similarly figure 4 shows the difference in the Eulerian velocity profiles in the wall layer. However, the separation at particle $\eta_s$ proceeds exactly as before: the spin of the sphere is brought to a halt but separation continues. At and beyond particle s, the Lagrangian velocity profiles with and without spin-down agree within $10^{-7}$.

The asymptotic description of the separating layer proceeds in the same manner as for the wall layer, with one distinction: the vertical position $y$ is now singular. The reason is evident from the integral (2.2), which turns singular in passing point s. The resolution, given in §3 of Part 1, is to refer $y$ to a reference position $y^+$ in the separating layer. Many definitions are possible for this reference, but a convenient example is

$$w(y^+,t) = 0.05 w(0,t). \tag{4.4}$$

For this definition $y^+$ corresponds to a typical boundary-layer thickness. The continuity equation (2.2) may now be written as

$$y = y^+ + \int_{\eta^+}^{\eta} \frac{\mathrm{d}\eta'}{x_{,\xi}(\eta',t)} \equiv y^+ + \tilde{y}, \tag{4.5a, b}$$

where $\tilde{y}$ is regular in the separating layer. Thus, when $y$ is replaced by $\tilde{y}$ and $v$ with $\tilde{v} = \dot{\tilde{y}}$, the description of the separating layer becomes of the same form (4.1), (4.2) as for the wall layer:

$$(x_{,\xi}, u_{,\xi}, w, \tilde{y}) = \sum_{n=0}^{\infty} \frac{1}{n!} |\delta t|^n (x_{,\xi}^{(n)}(\eta), u_{,\xi}^{(n)}(\eta), w^{(n)}(\eta), \tilde{y}^{(n)}(\eta)) \quad \text{for} \quad \eta > \eta_s, \tag{4.6a, b}$$

$$(u_{,x}, \tilde{v}, w) = \sum_{n=0}^{\infty} \frac{1}{n!} |\delta t|^n (u_{,x}^{*(n)}(\tilde{y}), \tilde{v}^{*(n)}(\tilde{y}), w^{*(n)}(\tilde{y})) \quad \text{for} \quad \tilde{y} = O(1). \tag{4.7a, b}$$

## 5. The emergence of logarithmic terms

In the previous two sections, the asymptotic expansions for the inner region and the wall and separating layers have been found. However, the position $y_s$ of the particle $\eta_s$ in the inner expansion, and the reference position $y^+$ in the separating layer remain undetermined.

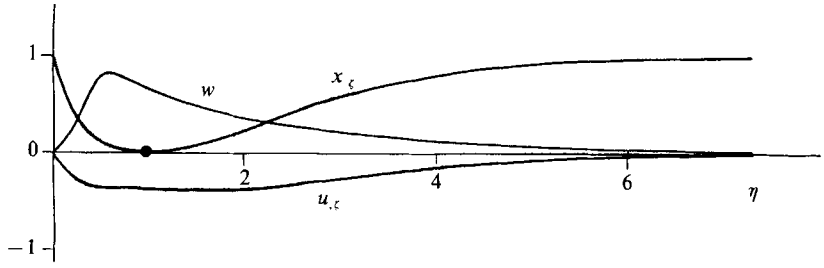


FIGURE 3. Lagrangian profiles when the spin of the sphere is smoothly brought to a halt. Comparison with the previous Lagrangian separation profiles, figure 1, shows that the velocity change generates a sublayer at the wall. However, this layer does not reach the particle $\eta_s$ in time to halt the separation process.

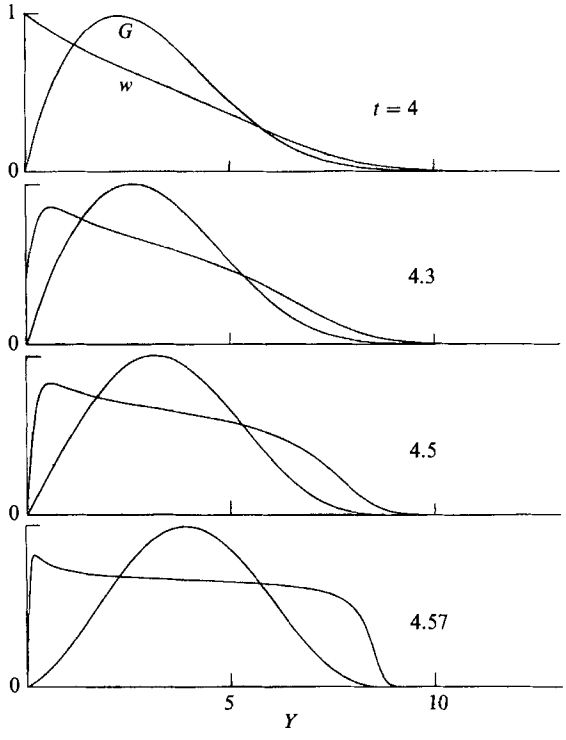


FIGURE 4. Eulerian profiles corresponding to figure 3.

To find $y_s$, the inner expansion (3.4), (3.5) can be matched with the wall layer (4.1), to yield

$$y_s(t) \sim \frac{\pi}{\beta|\delta t|^{\frac{1}{2}}} + 2B \ln \frac{1}{|\delta t|} + O(1), \tag{5.1}$$

where the coefficients $\beta$ and $B$ are given in (3.5*b*, *c*).

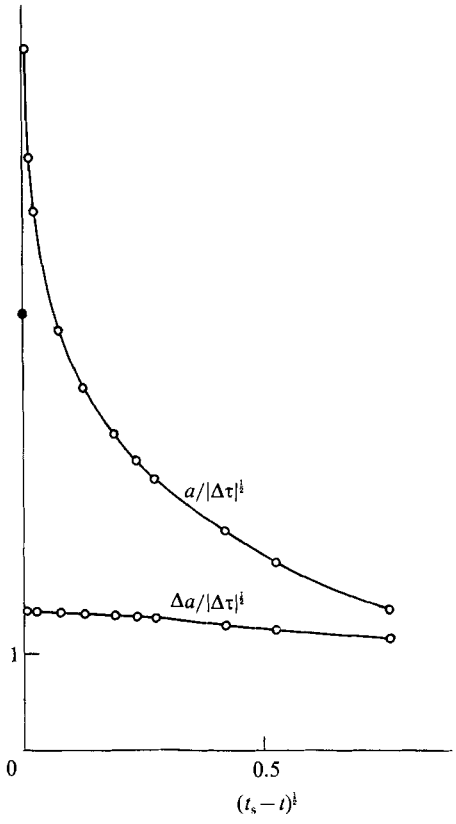


FIGURE 5. Presence of higher-order logarithmic terms in the expansions for the impulsively spun sphere. According to the original proposal of Banks & Zaturska (1979), the upper curve should linearly approach the value 4.6 indicated by the dot. But according to the present results the upper curve contains a logarithmic term, and only after subtraction of this term does the lower curve approach a constant value. See text for a comparison with the work of Simpson & Stewartson (1982).

The logarithmic term will lead to a corresponding logarithmic term in the Eulerian expansion of the velocity profile (3.6$a$), when rewritten in terms of $Y$:

$$G \sim \tfrac{1}{2}(1-\cos\beta Y)+\tfrac{1}{2}A\sin\beta Y+\ldots, \tag{5.2a}$$

$$A \sim -2\beta B|\delta t|^{\frac{1}{2}}\ln\frac{1}{|\delta t|}+(-2\beta B\ln(\tfrac{1}{2}(1-\cos(\beta Y))+A_0)|\delta t|^{\frac{1}{2}}, \tag{5.2b}$$

where $A_0$ is a constant depending on the wall layer profile.

The expansion originally proposed by Banks & Zaturska (1979) was of the same form (5.2$a$), but they proposed a different coefficient $A$, without the logarithmic term:

$$A_{\mathrm{BZ}} \sim 4.6|\delta t|^{\frac{1}{2}}.$$

To verify that there is in fact a missing logarithmic term, a numerical variable approximating $A$ was constructed as

$$a \equiv \frac{\pi}{2}\frac{Y_2-3Y_1}{Y_2-Y_1}, \tag{5.3a}$$

where $Y_1$ and $Y_2$ are the two $Y$-positions where $G = \frac{1}{2}$. For the Banks & Zaturska (1979) proposal $a \sim A_{\mathrm{BZ}} + O(|\delta t|)$, while for (5.2*b*)

$$a \sim -2\beta B|\delta t|^{\frac{1}{2}} \ln \frac{1}{|\delta t|} + O(|\delta t|^{\frac{1}{2}}). \tag{5.3b}$$

According to the present more accurate numerical results, the computed values for $a$ do not appear to approach the constant given by Banks & Zaturska (1979) (figure 5). If, however, the logarithmic term in (5.3*b*) is first subtracted from the curve, the required approach to a constant does become evident.

Simpson & Stewartson (1982) were the first to point out the presence of logarithmic terms based on an Eulerian description of the flow. However, our result $B = -0.3957$ agrees poorly with the value $-0.457$ found by Simpson & Stewartson (1982), who obtained their value from subtracting two large quantities and fitting of a straight line to the resulting smaller quantity. We submit that our value is independently supported both by the apparent convergence of the results in table 3, using the definitions in (3.5*b*, *c*), and also by its apparent success in eliminating the blow up of the curve figure 5.

With the inner solution now fully determined by (5.1), the position of the separating layer follows from matching its expansion for $y$, (4.5), (4.6), to the inner region (3.4), (3.5), (5.1). The matching requires

$$y^+ \sim \frac{2\pi}{\beta|\delta t|^{\frac{1}{2}}} + O(1). \tag{5.4}$$

The $O(1)$ constant is related to the arbitrariness in the possible definition of the reference position $y^+$ and the shape of the separation profiles in the wall and separating vorticity layers.

## 6. The first separated stages

Compared to the Eulerian computations, the most remarkable aspect of the Lagrangian computation is the absence of any numerical difficulties in the integration of the momentum equations near the initial separation time $t_{\mathrm{s}}$. The question arises of whether the Lagrangian solution continues to exist beyond this time. The numerical evidence in tables 1 and 3 and figures 6–8 indicates that a formal solution does indeed exist for a finite range of times $t_{\mathrm{s}} < t < t_{\mathrm{v}}$ beyond initial separation. Even at 1025 points across the boundary layer, there is no sign of convergence difficulties nor of instability. And theoretically, at least the coefficient of the second-order viscous derivatives in (2.1*b*) and (2.1*c*) remains positive, so that the time-like direction remains positive.

For these reasons we are led to assume that the Lagrangian boundary-layer problem does have a formal solution beyond initial separation. Whether such a formal solution has physical meaning is a second and separate question. Certainly at the equatorial plane itself, the separation must set up interactive processes which invalidate the further use of the original equations (2.1).

However, there is a second interpretation for the solution. Van Dommelen (1987) computed the Lagrangian solution to the full two-dimensional boundary layer around the sphere, a solution which also appears to remain regular at and beyond the separation time $t_{\mathrm{s}}$. Now, if it turns out that the interactive effects remain restricted to a small vicinity of the equator, say to $x = \frac{1}{2}\pi + O(Re^{-\alpha})$ with $\alpha > 0$, then the two

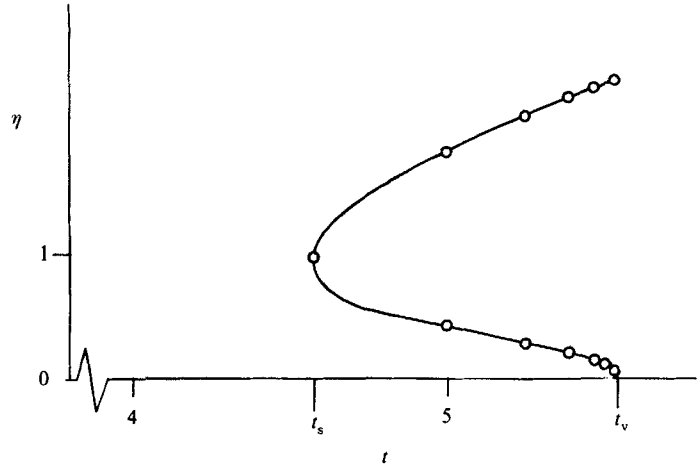


FIGURE 6. Trajectory of vanishing $x_{,\xi}$ for the impulsively spun sphere in the Lagrangian equatorial $(\eta, t)$-plane. In contrast to the Eulerian case, the Lagrangian solution does not appear to terminate at the time $t_s$ that separation starts. But near the settle-down time $t_v = 5.5476$ when the lower stationary point attaches itself to the wall, the Lagrangian solution turns singular also.

half boundary layers $x < \frac{1}{2}\pi$ and $x > \frac{1}{2}\pi$ would continue to describe the correct asymptotic limit away from the equator. These two half boundary layers would near $x = \frac{1}{2}\pi$ match with the small interactive region. The notion of a limited interaction region seems in line with steady descriptions (Stewartson 1958; Smith & Duck 1977), and the formation of an equatorial jet (Dennis & Ingham 1979; Dennis & Duck 1988). For a limited interaction region, the present solution describes the flow in the matching region $Re^{-\alpha} \ll |x - \frac{1}{2}\pi| \ll 1$ since it is the equatorial limit of the two-dimensional Lagrangian solution.

Whether or not these arguments apply, the boundary-layer equations are important enough by themselves that their possible behaviour is worth study. Note that a solution to the boundary-layer equations may be physically relevant in some settings even if it does not apply in other settings (cf. Smith 1982).

The initial characteristics of the continuity equation beyond time $t_s$ were found in §4.2, figure 3(i), of Part 1, and are such that the singular behaviour in the continuity equation remains restricted to $x = \frac{1}{2}\pi$. Because of the boundary conditions (2.1$g, j$) for $x_{,\xi}$, beyond time $t_s$ the single zero for $x_{,\xi}$ must separate into two zeros, at positions which will be denoted as $\eta_1$ and $\eta_2$. Computed values for $\eta_1$ and $\eta_2$ are given in table 3 and shown in figure 6. The two main boundary layers $x < \frac{1}{2}\pi$ and $x > \frac{1}{2}\pi$ each split into three layers near the equatorial plane. The layer of particles $\eta < \eta_1$ remains close to the wall. The middle layer of particles $\eta_1 < \eta < \eta_2$ penetrates relatively far from the wall on account of the strong growth in $y$ near $\eta_1$. The upper layer of particles $\eta > \eta_2$ penetrates still further from the wall because of the additional growth in $y$ near $\eta_2$. The middle layer further ejects a finite mass flow into the vicinity of the equatorial plane. It may be conjectured that this mass will develop into the equatorial jet.

## 7. The settle-down of the lower stationary point

When the time $t_v$ beyond the time $t_s$ of first separation is approached, new phenomena start to show up. The lower stationary point approaches the wall, figure

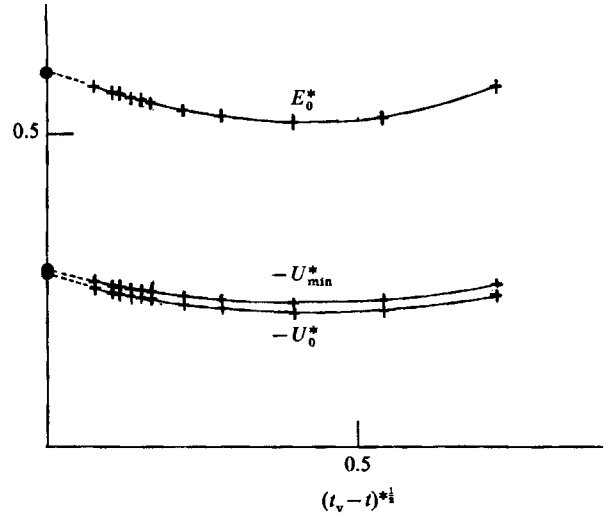


FIGURE 7. Behaviour of the Lagrangian solution when the settle-down time $t_v$ is approached. The scaled variables are defined in the text. The solid dots denote the values 0.5961, 0.2824, and 0.2745 according to the asymptotic solution, figure 9.

6, table 3, and the local value of the Lagrangian gradient $u_{,\xi}$ appears to blow up. Similarly the wall shear gradient $u_{,\xi\eta}$ rapidly increases, table 1. The 'settle-down' of the lower stationary point is depicted in figure 6. No significant singular behaviour is evident at the upper stationary point, cf. table 3.

Since an inviscid flow does not turn singular in the Lagrangian coordinate system, it is likely that viscous effects are a primary influence near settle-down. A balance of the viscous and convective terms in the Lagrangian boundary-layer equations (2.1) is consistent with an inner coordinate

$$E = \frac{\eta}{|\tau|^{\frac{1}{2}}}, \quad \tau \equiv t - t_v. \tag{7.1a, b}$$

Indeed the $E$-position $E_0$ of the lower stationary point appears to remain non-zero and finite near time $t_v$, figure 7. Since $x_{,\xi} = 1$ at the wall, and vanishes at the stationary point, the appropriate asymptotic expansion should be

$$x_{,\xi} \sim x_{,\xi}(E), \quad u_{,\xi} \sim \frac{U(E)}{|\tau|}. \tag{7.1c, d}$$

This agrees with figure 7, where the $U$-value $U_0$ at the stationary point and the minimum value $U_{\min}$ appear to remain finite. In addition the meridional wall shear gradient ($u_{xy}$ in Eulerian coordinates or equivalently $u_{,\xi\eta}$ in Lagrangian ones) should be of order $|\tau|^{-\frac{3}{2}}$. This may be verified independently of any estimated value for $t_v$ by examining whether the ratio $|u_{,\xi\eta}|^{\frac{3}{5}}/|u_{,\xi\eta}|^{\frac{3}{5}} = O(|\tau|^{-\frac{6}{5}})/O(|\tau|^{-\frac{3}{5}}) = O(1)$ remains finite. The numerical results shown in figure 8 do clearly support this. The correspondingly scaled Eulerian variables are

$$y = |\tau|^{\frac{1}{2}}Y, \quad u_{,x} = -\frac{G}{|\tau|}, \quad v = \frac{V}{|\tau|^{\frac{1}{2}}}. \tag{7.1e–g}$$

These viscous scalings are not to be confused with the inviscid ones of §3. The azimuthal velocity appears to approach a unit value, cf. $w_{,y}$ in table 1 and $w_1$ in table 3.

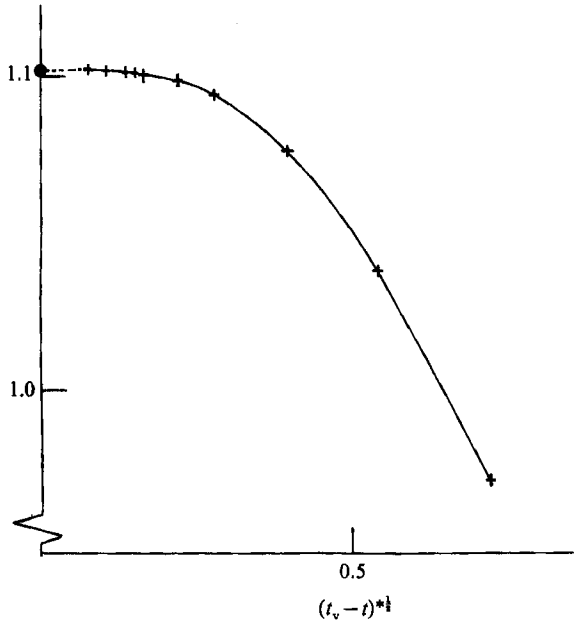


FIGURE 8. The agreement in wall shear with the asymptotic solution, figure 9, when the settle-down time $t_v$ is approached. The solid dot denotes the value 1.101615 according to the asymptotic solution, figure 9.

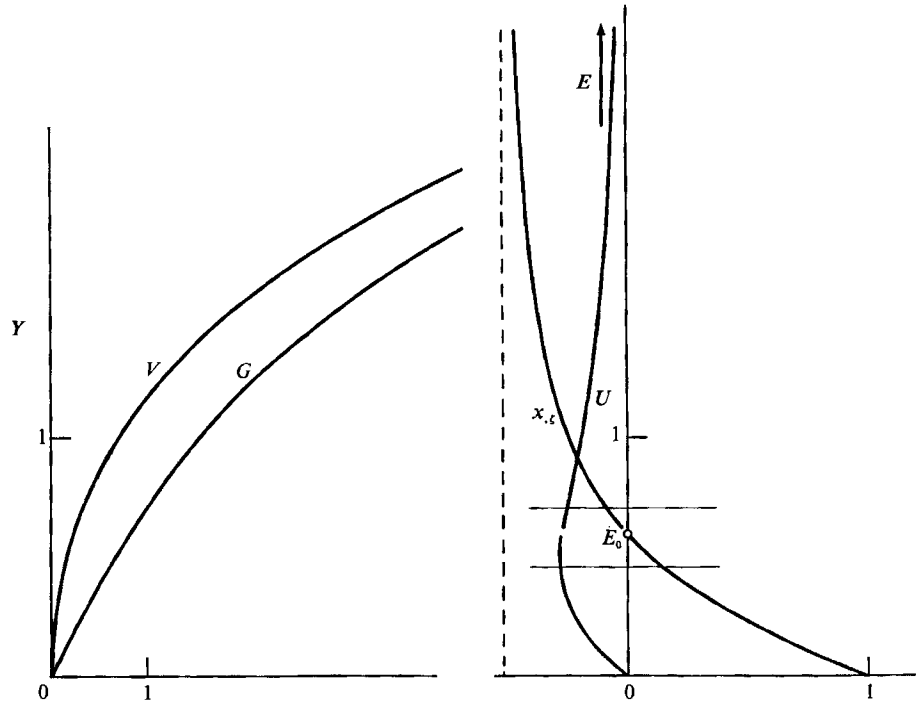


FIGURE 9. Proposed asymptotic solution in the vicinity of settle-down of the lower stationary point in figure 6. The Eulerian solution $0 \leqslant Y < \infty$ is equivalent to the lower Lagrangian solution $0 \leqslant E < E_0$.

| Solution | $x_{,\xi}$ | $x'_{,\xi}$ | $x''_{,\xi}$ | $U$ | $U'$ | $U''$ |
|---|---|---|---|---|---|---|
| $E < E_0$ | 0 | 0.92099 | 2.015 | −0.27450 | 0.13975 | 1.02 |
| $E > E_0$ | 0 | 0.92091 | 2.02 | −0.27450 | 0.13977 | 1.02 |

TABLE 4. First few Lagrangian derivatives of the solution figure 9 at the stationary point $E_0$

| | | | | | | | |
|---|---|---|---|---|---|---|---|
| 0 | −0.92 | $0.10\times10$ | −0.56 | −0.23 | 0.07 | 0.65 | $0.24\times10$ |
| $0.11\times10^{2}$ | $0.73\times10^{2}$ | $0.65\times10^{3}$ | $0.74\times10^{4}$ | $0.10\times10^{6}$ | $0.17\times10^{7}$ | $0.33\times10^{8}$ | $0.72\times10^{9}$ |
| $0.18\times10^{11}$ | $0.48\times10^{12}$ | $0.14\times10^{14}$ | $0.47\times10^{15}$ | $0.16\times10^{17}$ | $0.63\times10^{18}$ | $0.26\times10^{20}$ | $0.11\times10^{22}$ |
| $0.52\times10^{23}$ | $0.25\times10^{25}$ | $0.13\times10^{27}$ | $0.72\times10^{28}$ | $0.41\times10^{30}$ | $0.25\times10^{32}$ | $0.16\times10^{34}$ | — |

TABLE 5. Coefficients $C_n$ in the self-consistent Taylor series expansion (7.2) to the solution figure 9, for $n = 0, 1, \ldots, 30$. They show no evidence of a non-zero radius of convergence. The tabulated results do not depend critically on the precise values of $E_0$ and $C_1$.

Substitution of the inner expansion (7.1*a*, *b*) into the Lagrangian equations (2.1*a*) yields

$$U+\tfrac{1}{2}EU' = x_{,\xi}^2 U''-x_{,\xi}x'_{,\xi}U'+(x'^2_{,\xi}-x_{,\xi}x''_{,\xi})\,U, \tag{7.1h}$$

$$U = \tfrac{1}{2}Ex'_{,\xi}, \tag{7.1i}$$

where primes denote derivatives with respect to $E$. The equivalent Eulerian problem reads

$$G''-(V+\tfrac{1}{2}Y)\,G'+G^2-G = 0, \tag{7.1j}$$

$$G = V', \tag{7.1k}$$

where primes now denote derivatives with respect to $Y$. The Eulerian solution is only defined below the stationary point $E_0$.

Runge–Kutta solutions to the inner problems (7.1*h*, *i*) and (7.1*j*, *k*) are shown in figure 9. Briefly, the parts $0 \leqslant Y < \infty$ and $0 \leqslant E < E_0$ were found from upward shooting, and seeking the least singular solution. The part $E_0 < E < \infty$ was found from downward shooting, starting from a self-consistent asymptotic series truncated at the smallest term.

It is interesting to conjecture about the nature of the Runge–Kutta solution near the point $E_0$. In both Part 1 and in this paper, we have presented evidence in support of the assumption that the Lagrangian solution is regular at and beyond the time of initial separation $t_s$. Unless a further inner region exists, that would require that the Runge–Kutta solution is also regular at point $E_0$. This seems to agree with table 4, which shows that finite and unique values for the first few Lagrangian derivatives exist at $E_0$. In addition, for finite first derivative of $x_{,\xi}$ the self-consistent local expansion for the solution assumes the form of a Taylor series:

$$x_{,\xi} = \sum_n C_n(E-E_0)^n, \tag{7.2}$$

with the first 30 coefficients listed in table 5. When truncated at the smallest term, this series seems to give an excellent local approximation to the solution; it reproduces $x_{,\xi}$ and $U$ to four-digit accuracy within $0.458 < E < 0.7$. However, the coefficients in table 5 do not show evidence of a non-zero radius of convergence; the

| | | | | | | |
|---|---|---|---|---|---|---|
| $(t_v-t)^{*\frac{1}{2}}$ | 0.7218 | 0.5402 | 0.3953 | 0.2781 | 0.2180 | 0.1661 |
| | 0.1503 | 0.1326 | 0.1166 | 0.1030 | 0.0748 | — |
| $(t_v-t)^{\frac{1}{2}}$ | 0.7400 | 0.5455 | 0.3970 | 0.2786 | 0.2182 | 0.1661 |
| | 0.1503 | 0.1327 | 0.1166 | 0.1030 | 0.0748 | — |

TABLE 6. Comparison between the apparent time from settle-down as defined in (7.3) and the true value. (Mesh $1025 \times 0.003125$; $t_v = 5.54760$.)

series seems applicable in an asymptotic sense only. Whether the same non-convergence holds for the Lagrangian solution for $t_s < t < t_v$ is uncertain; only infinite values of the lower-order derivatives reflect numerical inaccuracy – non-convergence of the Taylor series around a point is not necessarily evident through reduced accuracy or convergence difficulties.

According to figures 7 and 8, the asymptotic solution of figure 9 is in good agreement with the numerical data. In both figures 7 and 8, in order to avoid the difficulty in choosing a precise value for time $t_v$, an apparent time difference $(t_v-t)^*$ was defined based on the asymptotic result $u_{,xy} = -G'(0)/|\tau|^{\frac{3}{2}}$. After differentiation with respect to time, this relation may be solved for $\tau$ to give the approximation

$$(t_v-t)^* \equiv \left(\frac{2|\dot{u}_{,xy}|}{3G'(0)}\right)^{-\frac{2}{3}}, \quad G'(0) = 1.277980908. \tag{7.3a, b}$$

Table 6 shows that this apparent time difference is in good agreement with the real time difference near time $t_v$ (which also provides more support for the applicability of the Runge–Kutta solution).

Summarizing the results, it would seem that the Lagrangian solution can be continued through separation until the lower stationary point reaches the wall. Beyond that time, the limiting singular behaviour of the main two boundary layers $x < \frac{1}{2}\pi$ and $x > \frac{1}{2}\pi$ near the equatorial plane can possible only be found from a complete integration of these layers.

## 8. Concluding remarks

Van Dommelen & Cowley (1990) showed that self-consistent unsteady separation processes can be derived by assuming a smooth Lagrangian solution. To give the strongest possible verification that this concept is physically meaningful, in this paper the equatorial boundary-layer separation for the impulsively spun sphere was recomputed. With only one spatial dimension, this case allows excellent numerical accuracy. Our scheme appears to be the most accurate yet; its separation time is accurate to seven digits before using Richardson extrapolation.

Even when we used over a thousand points across the boundary layer, we could not observe any deviations from the smooth Lagrangian solution proposed by Van Dommelen & Cowley (1990). Derivatives up to third order could easily be determined to five digit accuracy, cf. table 3. Derivatives of still higher order would be difficult to evaluate, but they play no significant part in the final separation structure. Moreover, singular behaviour of the higher-order derivatives would tend to render the evaluation of the lower-order derivatives more difficult, and we observed no evidence of that.

Numerical continuation of the boundary-layer solution beyond the time of first separation showed that the wall vorticity layer disappears in a finite time. Whether

a similar process occurs for the non-interactive solution of asymmetric two- or three-dimensional separation, in which the separation structure is in motion compared to the wall, remains unknown.

During parts of this investigation, the author was supported by the ONR, the AFOSR, and ICOMP, NASA Lewis.

## REFERENCES

BANKS, W. H. H. & ZATURSKA, M. B. 1979 The collision of unsteady laminar boundary layers. *J. Engng Maths* **13**, 193.

BANKS, W. H. H. & ZATURSKA, M. B. 1981 The unsteady boundary-layer development on a rotating disc in counter rotating flow. *Acta Mech.* **38**, 143–155.

BODONYI, R. J. & STEWARTSON, K. 1977 The unsteady laminar boundary layer on a rotating disk in a counter-rotating fluid. *J. Fluid Mech.* **79**, 669–688.

DENNIS, S. C. R. & DUCK, P. W. 1988 Unsteady flow due to an impulsively started rotating sphere. *Computers Fluids* **16**, 291–310.

DENNIS, S. C. R. & INGHAM, D. B. 1979 Laminar boundary layer on an impulsively started rotating sphere. *Phys. Fluids* **22**, 1–9.

ELLIOTT, J. W., COWLEY, S. J. & SMITH, F. T. 1983 Breakdown of boundary layers:, i. on moving surfaces, ii. in semi-similar unsteady flow, iii. in fully unsteady flows. *Geophys. Astrophys. Fluid Dyn.* **25**, 77.

SEARS, W. R. & TELIONIS, D. P. 1975 Boundary-layer separation in unsteady flow. *SIAM J. Appl. Maths* **28**, 215.

SIMPSON, C. J. & STEWARTSON, K. 1982 A note on a boundary-layer collision on a rotating sphere. *Z. Angew. Math. Phys.* **33**, 370.

SMITH, F. T. 1982 On the high Reynolds number theory of laminar flows. *IMA J. Appl. Maths* **28**, 207.

SMITH, F. T. & DUCK, W. 1977 Separation of jets or thermal boundary layers from a wall. *Q. J. Mech. Appl. Maths* **30**, 143.

STEWARTSON, K. 1958 On rotating laminar boundary layers. In *Boundary-Layer Research* (ed. H. Görtler), p. 57. Springer.

VAN DOMMELEN, L. L. 1981 Unsteady boundary-layer separation. PhD thesis, Cornell University.

VAN DOMMELEN, L. L. 1987 Computation of unsteady separation using Lagrangian procedures. In *Boundary-Layer Separation* (ed. F. T. Smith & S. N. Brown), p. 73. Springer.

VAN DOMMELEN, L. L. & COWLEY, S. J. 1990 On the Lagrangian description of unsteady boundary-layer separation. Part 1. General theory. *J. Fluid Mech.* **210**, 593–626.

VAN DOMMELEN, L. L. & SHEN, S. F. 1980 The spontaneous generation of the singularity in a separating laminar boundary layer. *J. Comput. Phys.* **38**, 125–140.

VAN DOMMELEN, L. L. & SHEN, S. F. 1982 The genesis of separation. In *Numerical and Physical Aspects of Aerodynamic Flows, Proc. Symp., Jan. 1981 Long Beach, California* (ed. T. Cebeci), p. 293. Springer.

VAN DYKE, M. 1975 *Perturbation Methods in Fluid Mechanics*, p. 86. Stanford: Parabolic.